

Voxel-CIM: An Efficient Compute-in-Memory Accelerator for Voxel-based Point Cloud Neural Networks

Xipeng LIN

The Hong Kong University of Science
and Technology(Guangzhou)
Guangzhou, China
xlin297@connect.hkust-gz.edu.cn

Shanshi Huang

The Hong Kong University of Science
and Technology(Guangzhou)
Guangzhou, China
shanshihuang@hkust-gz.edu.cn

Hongwu Jiang

The Hong Kong University of Science
and Technology(Guangzhou)
Guangzhou, China
hongwujiang@hkust-gz.edu.cn

ABSTRACT

The 3D point cloud perception has emerged as a fundamental role for a wide range of applications. In particular, with the rapid development of neural networks, the voxel-based networks attract great attention due to their excellent performance. Various accelerator designs have been proposed to improve the hardware performance of voxel-based networks, especially to speed up the map search process. However, several challenges still exist including: (1) massive off-chip data access volume caused by map search operations, notably for high resolution and dense distribution cases, (2) frequent data movement for data-intensive convolution operations, (3) imbalanced workload caused by irregular sparsity of point data.

To address the above challenges, we propose Voxel-CIM, an efficient Compute-in-Memory based accelerator for voxel-based neural network processing. To reduce off-chip memory access for map search, a depth-encoding-based output major search approach is introduced to maximize data reuse, achieving stable $O(N)$ -level data access volume in various situations. Voxel-CIM also employs the in-memory computing paradigm and designs innovative weight mapping strategies to efficiently process Sparse 3D convolutions and 2D convolutions. Implemented on 22 nm technology and evaluated on representative benchmarks, the Voxel-CIM achieves averagely $4.5\sim7.0\times$ higher energy efficiency (10.8 TOPS/w), and $2.4\sim5.4\times$ speed up in detection task and $1.2\sim8.1\times$ speed up in segmentation task compared to the state-of-the-art point cloud accelerators and powerful GPUs.

KEYWORDS

point cloud, compute-in-memory, neural network accelerator, map search

ACM Reference Format:

Xipeng LIN, Shanshi Huang, and Hongwu Jiang. 2024. Voxel-CIM: An Efficient Compute-in-Memory Accelerator for Voxel-based Point Cloud Neural Networks. In *IEEE/ACM International Conference on Computer-Aided Design (ICCAD '24), October 27–31, 2024, New York, NY, USA*. ACM, New York, NY, USA, 9 pages. <https://doi.org/10.1145/3676536.3676714>

Permission to make digital or hard copies of all or part of this work for personal or classroom use is granted without fee provided that copies are not made or distributed for profit or commercial advantage and that copies bear this notice and the full citation on the first page. Copyrights for components of this work owned by others than the author(s) must be honored. Abstracting with credit is permitted. To copy otherwise, or republish, to post on servers or to redistribute to lists, requires prior specific permission and/or a fee. Request permissions from permissions@acm.org.

ICCAD '24, October 27–31, 2024, New York, NY, USA

© 2024 Copyright held by the owner/author(s). Publication rights licensed to ACM. ACM ISBN 979-8-4007-1077-3/24/10...\$15.00
<https://doi.org/10.1145/3676536.3676714>

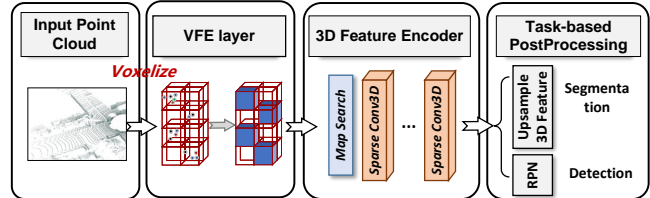


Figure 1: The generic network architecture of voxel-based algorithms for segmentation and detection tasks.

1 INTRODUCTION

The 3D point cloud is a mass of spatial points obtained from a variety of 3D sensors, such as LiDAR, cameras, etc., which serves as a fundamental role in various applications, ranging from VR/AR to autonomous vehicles and robotics. Unlike 2D images, the inherent complexity of point cloud data, characterized by its random and irregular spatial sparsity, poses huge challenges for point cloud processing algorithms.

In recent years, a variety of algorithms based on neural networks have been proposed to address these challenges [1–3]. Among them, the voxel-based network shows excellent performance [4–7]. Instead of handling huge amounts of irregular point data directly, the voxel-based network chooses to partition the continuous 3D space into volumetric pixels and voxelizes point data into structured formats. As shown in Fig. 1, a typical voxel-based network consists of three stages: voxel feature extractor (VFE), 3D Feature Encoder, and task-based postprocessing network. VFE layer is responsible for encoding the features of each voxel. The 3D Feature Encoder is composed of stacked Sparse 3D convolution (Spconv3D) operations. To facilitate Spconv3D, map search is conducted to avoid convolutions on empty voxels. For task-based postprocessing network, a region proposal network (RPN) is generally adopted to generate detection results (e.g., SECOND [5]) in detection tasks. And the Unet structure is usually used (e.g., MinkUnet [8]) in segmentation tasks. Despite showing excellent accuracy performance, the throughput of voxel-based networks is usually limited on traditional computing platforms such as GPU. (e.g. SECOND runs 36 FPS on Nvidia 3090ti and MinkUnet runs 13 FPS on Nvidia 2080ti [9]).

Although many efforts have been made to accelerate point cloud neural networks, there are still three main challenges that restrict the hardware performance of voxel-based networks. **1) The mapping operation is dominated by huge off-chip data access.** Map search, a classic operation prior to Spconv3D, aims to build IN-OUT maps to accelerate following Spconv3D. Previous acceleration

methods can primarily be divided into two categories, table-aided and table-free map search. Table-aided strategies used hash tables or octree-encoding-based tables, where all voxels are encoded [8–12]. Although table-aided methods can achieve $O(1)$ -level searching speed theoretically, The table requires a large storage capacity, potentially exceeding 100MB. On the other hand, The table-free strategies transform the search problem into an intersection-detecting problem, avoiding the huge table [13, 14]. However, this method introduces redundant off-chip memory access for input data. **2) Frequent data transfers for data-intensive computations.** In traditional Von Neumann architecture, the "memory wall" problem limits the processing speed of neural network calculations since massive data movement happens between the computing units and the storage units, resulting in low throughput [15]. Especially, both activations and weights need to be fetched from the storage unit. Moreover, most power consumed in conventional ASIC accelerators for DNNs is also from memory access operations. **3) Imbalanced workload caused by irregular sparsity of point data** [11, 16]. Due to the sparsity, randomness, and uneven distribution of point clouds, each weight corresponds to a different number of in-out pairs. Consequently, the computational workload is usually high for central weights while keeps low for weights on the edge. The gap between the workload of the central weights and the peripheral weights could be huge, leading to low computational resource utilization.

To address the above challenges, we propose Voxel-CIM, an efficient Compute-in-Memory (CIM) based accelerator for voxel-based neural network processing with a novel map search method. Our key contributions can be summarized as follows:

- To reduce the off-chip data access volume, we proposed a novel searching scheme, named by Depth-encoding-based Output Major Search (DOMS), which combines the output major searching approach and depth-encoding table. DOMS can maximize data reuse, achieving stable $O(N)$ -level off-chip memory access in various situations.
- We design a CIM processing unit and corresponding weight mapping strategies to process Spconv3D and Conv2D calculations efficiently. We also propose a weight workload balanced (W2B) method to solve the workload mismatch problem, which can realize a $2.3\times$ speedup in the segmentation benchmark.
- We comprehensively evaluate the performance of our proposed accelerator on detection and segmentation benchmarks, showing that our accelerator could achieve averagely $4.5\text{--}7.0\times$ higher energy efficiency (10.8 TOPS/w), and $2.4\text{--}5.4\times$ speedup in detection task and $1.2\text{--}8.1\times$ speed up in segmentation task compared to the state-of-the-art point cloud accelerators and powerful GPUs.

2 BACKGROUND

A. Map Search Operation

Map search is a critical operation to accelerate subsequent sparse convolution by building the IN-OUT maps. We define the input and output voxel points as P_i and Q_j , where $P_i, Q_j \in \mathbb{Z}^3$ are the quantized coordinates in Z-dimensional space. For each output point

Q_j , we need to traverse all its adjacent locations with kernel offsets $\Delta^3(K)$ (K is the size of kernel, e.g., $\Delta^3(3) = \{-1, 0, 1\}^3$). Each valid pairs of input point P_i and output point Q_j constitutes one item in the IN-OUT maps, defined as $\mathcal{M}(j) = \{(P_i, Q_j, W_\delta) | \delta \in \Delta^3(K)\}$. This map will guide subsequent sparse convolutions, thereby avoiding performing convolutions on empty voxels [17].

B. Sparse 3D Convolution

A sparse tensor representation consists of two parts: the voxels' spatial coordinates and feature vectors. Mathematically, the collection of sparse tensors T of one layer can be represented as:

$$P = \begin{bmatrix} x_1 & y_1 & z_1 \\ \vdots & \vdots & \vdots \\ x_N & y_N & z_N \end{bmatrix} P_i \in \mathbb{Z}^3, \quad F = \begin{bmatrix} f_1^T \\ \vdots \\ f_N^T \end{bmatrix} f_i \in \mathbb{R}^C \quad (1)$$

where $P_i = (x_i, y_i, z_i)$ is the coordinates of the non-zero voxel, f_i is the associated feature vector, and N is the number of non-zero voxels. For a sparse 3D convolution with a kernel size K applied to a sparse tensor T , the output feature at coordinate Q_o is:

$$f'_o = \sum_{\delta \in \Delta^3(K)} W_\delta f_i, \quad \text{for } (P_i, Q_o, W_\delta) \in \mathcal{M}(o) \quad (2)$$

where f'_o is the output feature at coordinate Q_o , and $\mathcal{M}(o)$ represents all in-out pairs associated to the output coordinate Q_o .

There are three different kinds of Spconv3D as follows:

- *Submanifold Spconv.* The submanifold spconv preserves the spatial location of voxel data, and is typically used for spatial feature embedding in the middle of a block. The common parameter setting includes a kernel size of 3 and a stride of 1, denoted as subm3.
- *Generalized Spconv.* The generalized spconv is often positioned at the end of a block as a downsampling layer. It operates under a scheme where an output is considered valid if any inputs fall within the kernel range. Consequently, the output tends to be more dispersed in spatial distribution. The typical parameter setting includes a kernel size of 2 and a stride of 2, denoted as gconv2.
- *Transposed Spconv.* The transposed spconv is essentially the reverse process of the generalized spconv and is commonly employed for upsampling in segmentation tasks. It follows the same computational rules as the generalized spconv.

C. Region Proposal Network

RPN is widely used in detection frameworks [18, 19], which deals with dense and structured tensor features to generate the final detection results. Typically integrated with a pyramid structure [20], an RPN comprises three blocks of stacked 2D convolution (Conv2D) layers. Each block downsamples the feature map with a stride of 2. The last two blocks upsample their features and concatenate them with those of first block. Then the concatenated feature is used for subsequent detection.

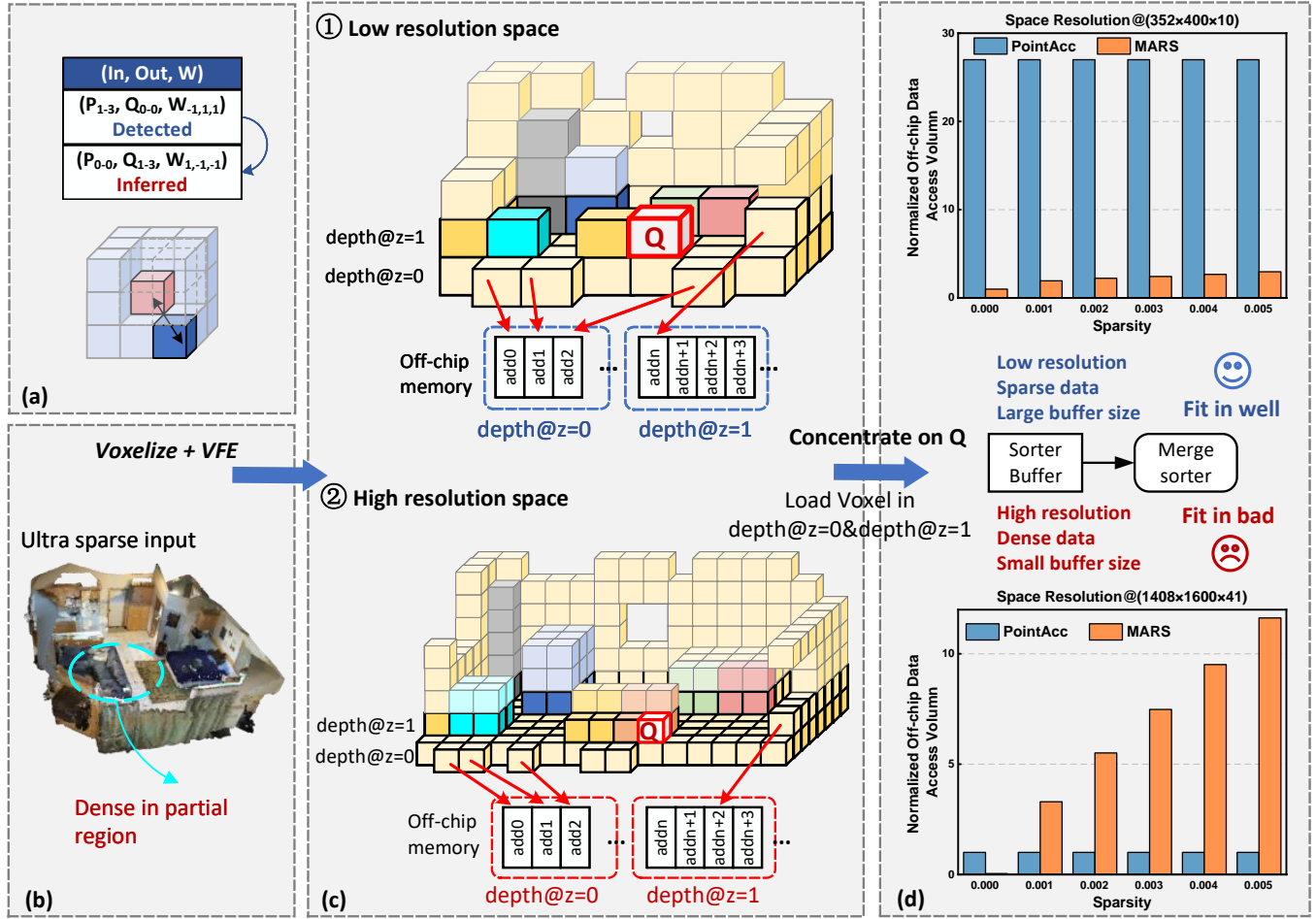


Figure 2: (a) The reverse mapping pairs can be inferred due to symmetry. (b) The visualization of input cloud data. (c) Voxelization with low resolution VS. voxelization with high resolution. (d) The comparison of normalized off-chip data access volume in various situations. (To simulate buffer limitations in extreme cases, we set the buffer size to match the length of the merger sorter, which is 64.)

3 VOXEL-CIM ACCELERATOR DESIGN

3.1 Effective Depth-encoding-based Output Major Searching Method

A. Previous Methods

Previous table-free map search methods can be divided into two categories, weight-major approach and output-major approach.

Weight-major Approach. This approach is proposed by PointAcc [13]. It iterates and loads all voxels for each weight to find intersection pairs. The on-chip buffer is not large enough to hold all voxels at a time, which causes redundant memory access. If it has N voxels and the 3D convolution kernel with size K , the off-chip memory data access volume can reach up to $O(K^3 \times N)$.

Output-major Approach. This approach is proposed by MARS [14]. It concentrates on each output voxel, maximizes voxel reuse, and achieves $O(N)$ for off-chip memory access theoretically. It also utilizes the symmetry of the conv3D kernel to reduce half of the

mapping calculation. As shown in Fig. 2(a), the $3 \times 3 \times 3$ kernel is central symmetry. If pair $(P_{1-3}, Q_{0-0}, W_{-1,1,1})$ exists, a reserve mapping pair $(P_{0-0}, Q_{1-3}, W_{1,-1,-1})$ must exist. This implies that instead of searching the 26 surrounding positions, it is sufficient to examine half adjacent positions, merely 13.

To ensure that exhaustively search all possible in-out pairs for each output with a single load, it must be able to accommodate two depths' voxels at least, which raises the size requirement for sorter buffer. As depicted in Fig. 2(c) ①, for the output voxel Q , the searching space is restricted to two depths (depth@z=0 and depth@z=1, marked in darker color). In most cases, the voxel space is ultra sparse, and the sorter buffer is sufficient to hold the voxels of two depths. However, there can be dense distributions in some partial regions, as shown in Fig. 2(b). What's worse, with the introduction of simpleVFE [21] and the application of complex scenarios, the network tends to perform Spconv3D on high-resolution voxel spaces. As illustrated in Fig. 2(c) ②, voxelization with high resolution will

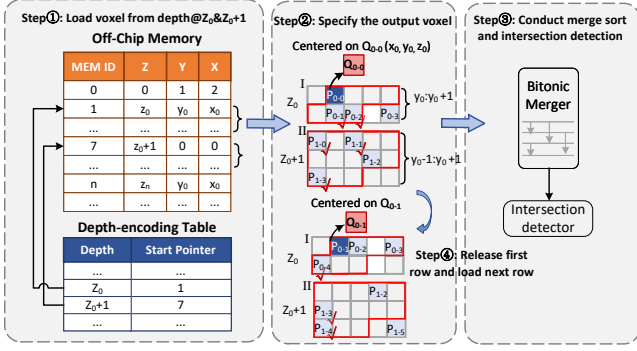


Figure 3: The workflow of DOMS

generate large scale voxel space to keep detailed surrounding information. If the sorter buffer is not enough to store two depths' voxels, this method will require multiple loading to exhaustively search all space for one output. As illustrated in Fig. 2(d), when the search space is low resolution, the data distribution is very sparse, and the sorter buffer is large enough, MARS can realize optimal $O(N)$ access. If the search space is high resolution and the data distribution is dense relatively, the data access volume deteriorates rapidly due to buffer limitation and repeated loading.

B. Insight

The essential problem is that voxels' size of two depths is still too large to fit in the sorter buffer and merge sorter circuit in extreme cases. Actually, there is no need to accommodate voxels of two continuous depths. As shown in Fig. 3, for an output voxel $Q_{0,0}(x_0, y_0, z_0)$, the valid searching space is restricted to two consecutive rows ($z_0, y_0 : y_0 + 1, z_0$) at the same depth and three consecutive rows ($z_0, y_0 - 1 : y_0 + 1, z_0 + 1$) at the next adjacent depth. If the position of start voxel of each depth can be located in off-chip memory, we can load the voxels of corresponding depth directly. Thus, we can build a depth-encoding table to record the start pointer of each depth in off-chip memory. For each output voxel, we can locate the start position of corresponding depth, and tile two rows of the same depth and three rows of the next depth to ensure complete searching space.

C. Depth-encoding-based Output Major Search

Fig. 3 illustrates the tiling and scheduling strategy. Assuming that each depth's buffer can hold only 4 voxels, the search process is as follows: **Step①**: In the beginning, the voxels of first two depths (z_0 and $z_0 + 1$) are tiled to corresponding buffer (I and II) respectively as many as possible; **Step②**: Specify the output voxel and calculate its 13 adjacent positions by adding kernel offset; **Step③**: Pack two depths' voxel and output adjacent positions to merge sorter, and detect intersection; **Step④**: Then, the data of first row of two buffer (I : $P_{0,0}@z_0$ and II : $P_{1,0}, P_{1,1}@z_0 + 1$) will be released and the data of margin rows (I : $P_{0,1}, P_{0,2}, P_{0,3}@z_0$ and II : $P_{1,2}, P_{1,3}@z_0 + 1$) will be reused for next search. For the output of next row, we need to load data of next row (I : $P_{0,4}@z_0$ and II : $P_{1,4}, P_{1,5}@z_0 + 1$) for processing. Keep processing until the entire depth is fully handled. After completing the search of the depth@ z_0 ,

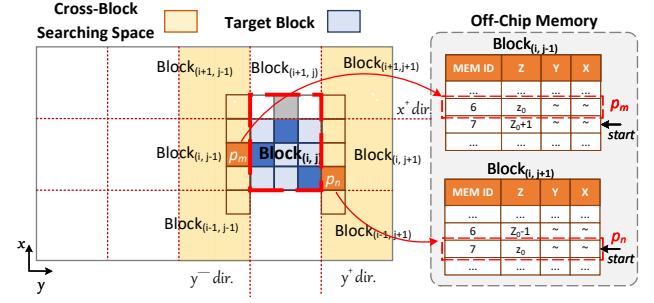


Figure 4: Block-DOMS. Voxels of neighboring blocks in y^- and y^+ direction (yellow regions) can be easily located by depth-encoding tables. Voxels of the neighboring block in the x^+ direction can be copied to $Block_{(i,j)}$.

Algorithm 1: Searching Space Confirmation Algorithm

```

Input: Block sets:  $\mathbb{B} = \{(m, n) | (m, n) \in \mathbb{D}^2\}$ ,  

Depth-encoding table set:  $\{T_{(m,n)} | (m, n) \in \mathbb{B}\}$ , Input  

Voxels:  $\{P_k^{(m,n)} | P_k^{(m,n)} = (x_k, y_k, z_k), (m, n) \in \mathbb{B}, k = 1, 2, \dots, N_b\}$ ,  

Output Voxel:  $Q_0^{(i,j)} = (x_0, y_0, z_0), (i, j) \in \mathbb{B}$   

Output: Search Space  $\mathbb{S}_0$   

1 Initialization:  $\mathbb{S}_0 \leftarrow \emptyset$ ;  

2  $\mathbb{S}_0 \leftarrow \mathbb{S}_0 \cup \{P_k^{(i,j)} | y_k = y_0 : y_0 + 1, z_k = z_0\}$ ;  

2 # Traverse the three neighbor blocks in  $y^-$  dir.  

3 foreach  $\Delta_x$  in  $\{-1, 0, +1\}$  do  

4   if  $(x_0 + \Delta_x, y_0 - 1, z_0)$  in  $Block(i + \Delta_x, j - 1)$  then  

5     # Locate via  $T_{(i+\Delta_x, j-1)}$   

6      $\mathbb{S}_0 \leftarrow \mathbb{S}_0 \cup \{P_k^{(i+\Delta_x, j-1)} | y_k = y_0 - 1, z_k = z_0\}$ ;  

6      $\mathbb{S}_0 \leftarrow \mathbb{S}_0 \cup \{P_k^{(i+\Delta_x, j-1)} | y_k = y_0 - 1, z_k = z_0 + 1\}$ ;  

7 # Traverse the three neighbor blocks in  $y^+$  dir.  

8 foreach  $\Delta_x$  in  $\{-1, 0, +1\}$  do  

9   if  $(x_0 + \Delta_x, y_0 + 1, z_0)$  in  $Block(i + \Delta_x, j + 1)$  then  

10    # Locate via  $T_{(i+\Delta_x, j+1)}$   

11     $\mathbb{S}_0 \leftarrow \mathbb{S}_0 \cup \{P_k^{(i+\Delta_x, j+1)} | y_k = y_0 + 1, z_k = z_0\}$ ;  

11     $\mathbb{S}_0 \leftarrow \mathbb{S}_0 \cup \{P_k^{(i+\Delta_x, j+1)} | y_k = y_0 + 1, z_k = z_0 + 1\}$ ;  

12 return  $\mathbb{S}_0$ 

```

the target output moves to depth@ $z_0 + 1$. The buffer I will be cleared, and new voxels in depth@ $z_0 + 2$ will be loaded.

With the assistance of DOMS, our buffer only needs to hold a portion of corresponding depth. However, each depth's voxels need to be loaded twice (once for the target in previous depth and once for the target in current depth), resulting in $O(2N)$ memory access. If the FIFO buffer is large enough to hold voxels of the entire depth, the release of the voxels in depth@ $z_0 + 1$ could be avoided at **Step④**, which can realize $O(N)$ for memory access.

D. Blocked Depth-encoding-based Output Major Search

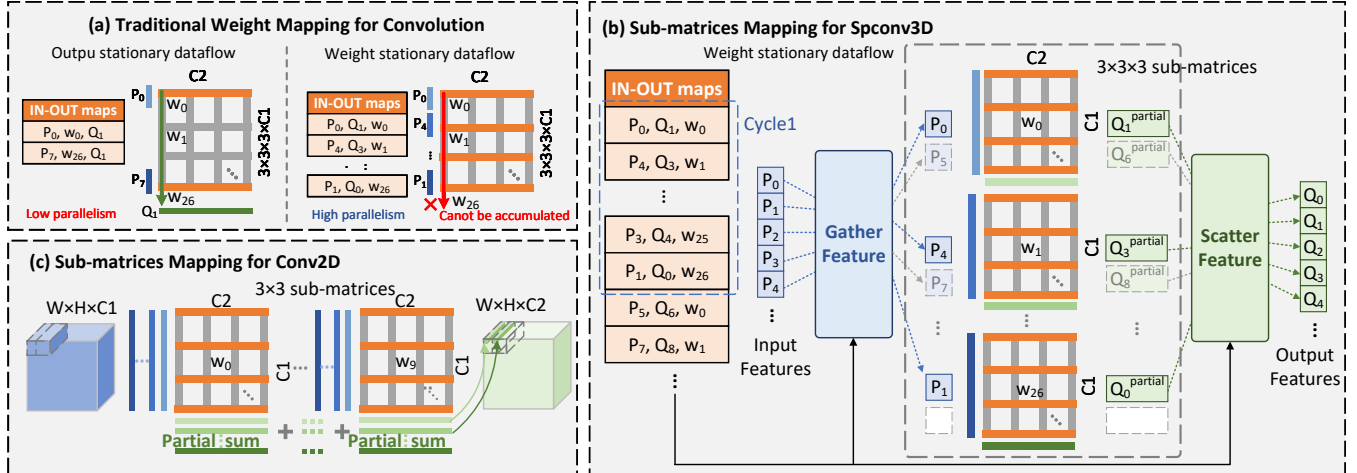


Figure 5: (a) Traditional weight mapping method for convolution (b) Sub-matrices mapping method for Spconv3D (c) Sub-matrices mapping method for Conv2D (Take K=3 as an example)

Furthermore, to achieve stable $O(N)$ memory access volume in various situations, we propose block-DOMS. This method divides the voxel space into 2D grids to downsize each depth. After data is re-organized at the memory, the dominant obstacle lies in how to conduct cross-block search efficiently. As the example shown in Fig. 4, for the output voxel in $Block_{(i,j)}$ (blue region), the adjacent voxels from neighbor blocks in $y^-dir.$ and $y^+dir.$ (yellow regions) can be easily located in memory by depth-encoding tables, which must be located at the beginning or end of each depth. But the adjacent voxels from neighbor block in $x^+dir.$ are hard to be located and the entire depth need to be loaded for further searching. To address this problem, we copy the adjacent voxels from neighbor block ($Block_{(i+1,j)}$) and save them in $Block_{(i,j)}$, to avoid cross-block searching in $x^+dir.$. The $x^-dir.$ doesn't need to be considered due to symmetry. Experiments show that the replicated voxels only account for less than 6% of all voxels, which is negligible. The detailed Searching Space Confirmation algorithm is shown in Alg. 1. Each block needs a depth-encoding table. Hence, there is a trade-off between table size and searching efficiency.

3.2 Weight Mapping Strategies for CIM Unit

CIM is emerging as an efficient paradigm to address the memory wall bottleneck. The weights can be stored in the crossbar-like memory arrays and inputs can activate multiple rows. Thus, the multiply-and-accumulate (MAC) operations can be performed in parallel, which significantly reduces the massive data access. Previous CIM-based DNN accelerators only focused on dense Conv2D operations, mainly used in 2D image applications [22–25]. There are no attempts to accelerate Spconv3D with CIM architecture before. In this section, we propose a CIM-based computing unit, which can support both Spconv3D and Conv2D operations flexibly.

A. Weight Mapping Methods for Spconv3D & Conv2D

In traditional weight mapping method for CIM-based accelerators, every channel of the kernel is unrolled into a long column and mapped into a column of memory array. The value in *column-axis*

will be accumulated to get output features. As illustrated in Fig. 5 (a), for a typical subm3's kernel with size $C1 \times K \times K \times K \times C2$, every channel ($C1 \times K \times K \times K$) is unrolled into a long column, $C2$ columns in total. In this mapping method, the input features of each cycle will be multiplied by the weights and accumulated to get the identical feature tensor. However, this mapping method doesn't support Spconv3D operations efficiently. In Spconv3D operations, if we use output stationary dataflow, we will waste lots of CIM computational resources due to low parallelism caused by input's sparsity; if use weight stationary dataflow, the in-out pairs for each weight correspond to different outputs and cannot be accumulated. Therefore, we need to design a more efficient weight mapping method for Spconv3D.

Inspired by [26], we propose a sub-matrices mapping method for Spconv3D. The weights at different kernel locations are mapped into different sub-matrices. As shown in Fig. 5 (b), for subm3's kernel with size $C1 \times K \times K \times K \times C2$, there will be $K \times K \times K$ sub-matrices, and each sub-matrix will have a size of $C1 \times C2$. This method allows each weight to be independently controlled for activation or idling, providing more flexible support for Spconv3D. To maximize the utilization of CIM parallel computational resources, we adopt the weight stationary dataflow. 1) In each cycle, the gather unit will gather all features for all weights of this layer as much as possible according to IN-OUT maps info. 2) Then, the input features will be multiplied with associated weights. 3) Scatter and accumulate the partial sum to corresponding output feature tensor according to IN-OUT maps. To maximize the feature reuse, the input batch of each cycle will be selected based on the principle of maximizing overlap with the batch of last cycle.

For Conv2D operations in RPN, because the input feature map has structured tensor format in spatial locations, we use the same sub-matrices mapping method to maximize the feature reuse. As shown in Fig. 5 (c), for a typical Conv2D kernel with size $C1 \times K \times K \times C2$, there will be $K \times K$ sub-matrices, and each sub-matrix will have a size of $C1 \times C2$. In this method, the input feature vectors of the current sub-matrix can be reused for next sub-matrix in next

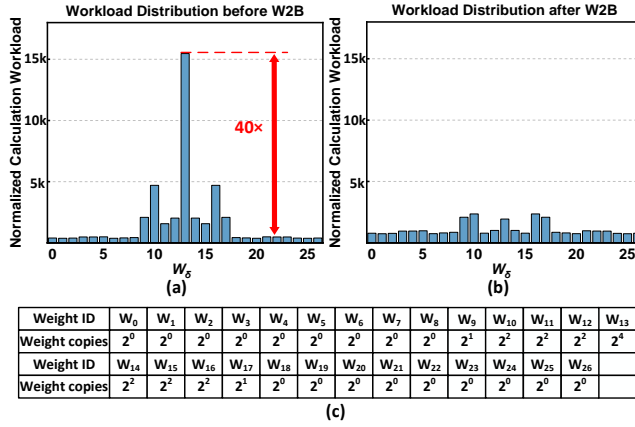


Figure 6: (a) The workload distribution shows a huge imbalance before W2B. (b) The workload imbalance is alleviated after W2B. (c) Parameter setting of W2B for the first layer (subm3) of SECOND.

cycle, when the kernel is sliding on input feature maps. Hence, it can maximize feature reuse.

B. Weight Workload Balanced Method

In traditional CIM unit, all weights are evenly mapped into memory cells. This mapping paradigm is not suitable for computations of irregular point cloud data. As shown in Fig. 6 (a), different weights correspond to varying number of in-out pairs, the workload gap between the central and the peripheral weights can even more than 40 times. Once the computational workload for peripheral weight computing units is completed, only the central weight computing unit remains active, which leaves the peripheral weights stay idle. This results in a considerable underutilization of computational resources. To balance the computational workload of different weights, we replace the evenly distributed weight mapping paradigm with the weight workload balanced (W2B) method. Extra copies are made to the central weights, while the edge weights are either not replicated or replicated to a lesser extent. The Fig. 6 (c) is an optimization example of detailed copying factor parameter setting for the first layer (subm3) in SECOND. The weight's workload is evaluated by normalized computational workload, defined by workload/weight copies. After optimization, the workload distribution becomes more uniform (Fig. 6 (b)).

3.3 Overall Architecture

As shown in Fig. 7, Voxel-CIM is mainly composed of two main cores: map search core and computing core. The map search core realizes DOMS and block-DOMS operations for efficient kernel map search. It uses two voxel FIFO buffers (I and II) to store the voxels across two adjacent depths. The voxel coordinates are loaded to the corresponding buffer row by row according to the depth-encoding table. Upon loading, the output voxel coordinates are calculated, and its adjacent positions are determined by adding the kernel offset by a parallel adder. The merge sorter is a bitonic sorter designed for fixed-length sequences. The intersection detector is implemented using a comparator that compares three coordinates

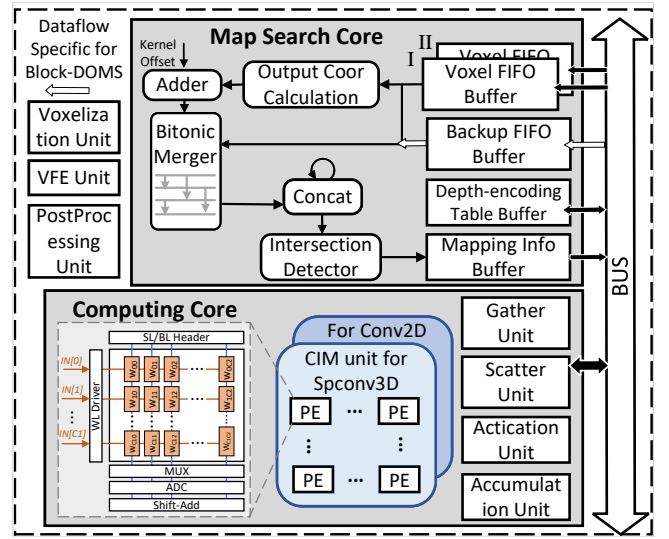


Figure 7: Overview of Voxel-CIM architecture.

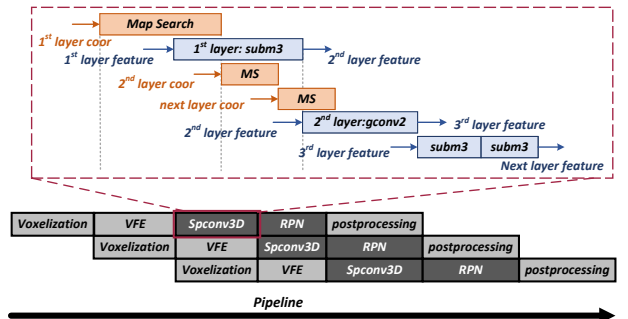


Figure 8: MS-wise pipeline and Compute-wise pipeline.

simultaneously in parallel. Valid in-out pairs are temporarily stored in the Mapping Info buffer. To activate block-DOMS, the backup FIFO buffer is hired to store the voxel coordinates from neighbor blocks.

In the computing core, a set of CIM units is used to conduct Conv2D and Spconv3D by corresponding weight mapping strategies. The CIM unit is composed of tiles, where each tile contains 1024×1024 memory cells. Each cell can store 1 bit information. The tile is divided into different PEs. Each PE contains all necessary resources to perform MAC operations, such as MUXs, ADCs, Shift-Adders, etc. According to sub-matrices mapping method, the weight's matrices are mapped to memory in units of PE.

In addition, the voxelization unit is used to partition the point cloud into different voxels in the initial stage. The VFE unit can support various VFE operations (e.g., dynamic VFE and simple VFE) flexibly. The post-processing unit is responsible for subsequent processing work, targeting different tasks.

Fig. 8 shows the hybrid pipeline for detection tasks, containing MS-wise pipeline and compute-wise pipeline. The Map Search Core follows the MS-wise pipeline: the map search (MS) for 2nd layer

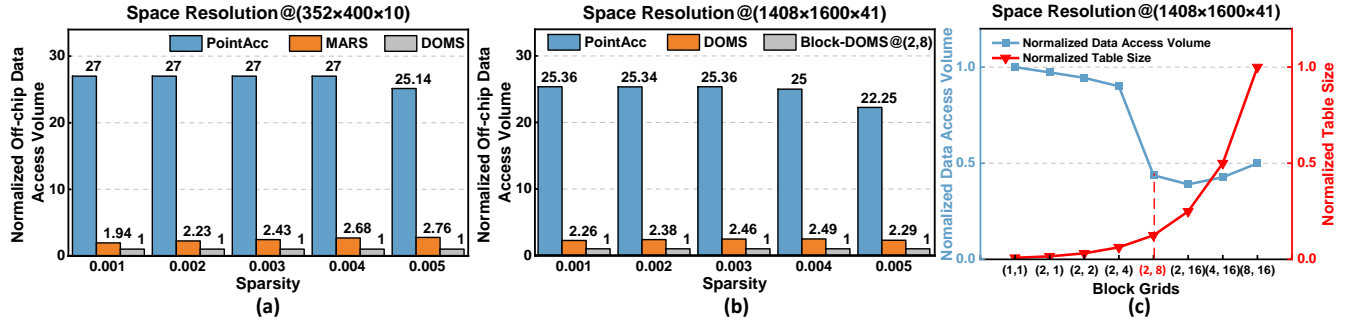


Figure 9: (a) Normalized data access volume comparison in low space resolution. (b) Normalized data access volume comparison in high space resolution. (c) Trade-off between data access volume and table size.

does not depend on the results of the 1st layer’s convolution; therefore, as soon as the MS for 1st layer is complete, the 2nd layer’s MS can commence immediately. The computing core follows the compute-wise pipeline: the 1st layer’s convolution does not require the completion of its entire map search; it can be executed as long as there are a sufficient number of in-out pairs. The 2nd layer’s compute needs to wait the completion of 1st layer. Two consecutive subm3 layers share common IN-OUT maps, without changing the position of voxels, thus the latter subm3 layer doesn’t require MS again.

4 EVALUATION

A. Evaluation Setup

Table 1: EVALUATION BENCHMARKS

Application	Dataset	Model	Notation
Detection	KITTI[27]	SECOND[5]	Det
Segmentation	SemanticKITTI[28]	MinkUNet[8]	Seg

Benchmarks. We choose 2 classic voxel-based networks, SECOND [5] and MinkUNet [8] to evaluate performance on detection and segmentation tasks respectively, as shown in Table 1. Experiments are conducted on 2 widely used benchmarks, KITTI and SemanticKITTI. Like [9], all weights of models are quantized to 8 bits.

Hardware Simulation. To evaluate the performance of map search methods, we developed a simulator based on Python. This simulator can generate random voxel data with varying space resolution and sparsity according to our setting. The behavior of searching methods will be modeled to analyze the off-chip data access volume and sorting times. The hardware performance of Voxel-CIM architecture is evaluated with NeuroSim framework [29]. The overhead of other units such as Voxelization, VFE etc. are evaluated on Xeon Platinum 8358P CPU.

Baseline. Several representative hardware platforms are selected as baselines, including four start-of-the-art Spconv-based accelerators and two powerful Nvidia GPUs. Standard networks, such as

SECOND and MinkUNet, are implemented on NVIDIA GPU and Xeon CPU to evaluate the overall end-to-end performance.

B. Evaluation Results

1) Comparison of Map Search Methods.

To analyze the limitation of the sorter buffer, we set the buffer size to match the length of merge sorter, that is 64. Fig. 9 shows our simulation results with varying space resolution and sparsity cases. When the space resolution is low (e.g. 352 × 400 × 10), both MARS and DOMS show superiority to PointAcc. But with the sparsity increases, the data access volume of MARS increases slightly while DOMS shows stable optimal performance with $O(N)$ access. When the space resolution is high (e.g. 1402 × 1600 × 41), the data access volume of DOMS also increases slightly, nearly to $O(2N)$. Accordingly, we employ block-DOMS to optimize the searching process.

To find a ideal block partition factor, we analyze the depth-encoding table size and data access volume with fixed sparsity@0.005. As shown in Fig. 9(c), smaller block granularity tends to result in less data access volume, yet the size of the table increases accordingly. Additionally, when the number of blocks reaches a certain threshold, data access volume may increase due to the replicated voxel in $x + dir$. Given the trade-off between data access volume and table size, the most optimal block partition factor is (2, 8) for this specific case. As illustrated in Fig. 9(b), it is obvious that the block-DOMS@(2,8) can maintain $O(N)$ data access volume in various situations.

2) Weight Workload Balanced Method.

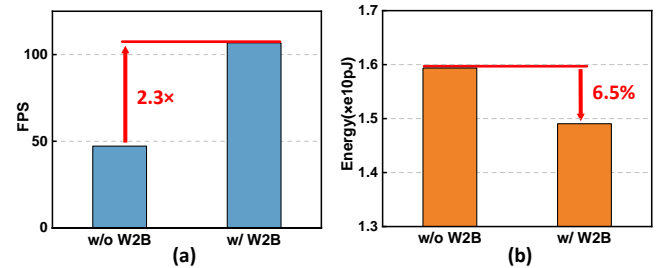


Figure 10: Performance improvement with W2B in terms of FPS and energy consumption for segmentation task.

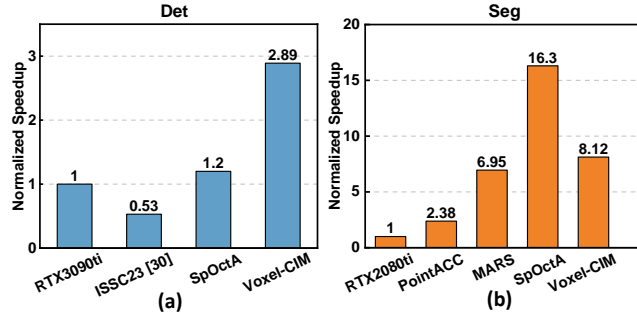


Figure 11: Normalized speedup compared to previous works and powerful GPU in detection and segmentation tasks.

Table 2: COMPARISON WITH OTHER WORKS

Chip	PointACC [13]	MARS [14]	ISSCC23 [30]	SpOctA [9]	Voxel-CIM
Tech (nm)	40	40	28	40	22
Frequency (MHz)	1000	1000	450	400	1000
Buffer (KB)	776	776	176	177.4	776
DRAM Bandwidth	HBM2 250GB/s	HBM2 250GB/s	-	DDR4 16GB/s	HBM2 250GB/s
Peak Throughput (TOPS)	8000	8000	225	200	27822
Peak Energy Efficiency(TOPS/W)	-	-	1.55@0.85V	2.39@1V	10.8@0.85V
Det(fps)	-	-	19.4	44.0	106
Seg(fps)	31.3	91.4	-	214.4	107

We propose the W2B method to solve the weight workload imbalance problem in Spconv3D. The experiments are conducted on MinkUnet for segmentation tasks because the segmentation network primarily consists of Spconv3D layers. The experiment results are shown in Fig. 10. After W2B, the imbalance issue has been mitigated, achieving a 2.3× speedup and 6% decrease in energy consumption.

3) Comparison with the State-of-the-Art Works

The implementation details and overall performance are summarized in Table 2. Voxel-CIM is implemented using 22 nm technology and operates at a frequency of 1000MHz. The CIM component is based on SRAM memory cells. The Voxel-CIM achieves a peak throughput of 27.8 TOPS. Compared to other Spconv-based accelerators, the Voxel-CIM achieves 10.8 TOPS/W @ 0.85V, showing 4.5~7.0× higher energy efficiency. As shown in Fig. 11, for object detection task in KITTI benchmark, the Voxel-CIM achieves 2.89× speedup over a powerful GPU 3090ti, and 2.4× speed up over the state-of-the-art works. For segmentation task in SemanticKITTI benchmark, our accelerator achieves 8.12× speedup over a powerful GPU 2080ti. Although it is slower than the state-of-the-art work in terms of FPS, it offers a 4.5× higher energy efficiency.

5 CONCLUSION

In this paper, we propose Voxel-CIM, a Compute-in-Memory (CIM) based accelerator for voxel-based neural network processing. The novel map search methods, DOM and block-DOMS, are proposed to reduce off-chip memory access volume, achieving stable $O(N)$ -level data access volume in various extreme situations. We also design dedicated weight mapping methods to efficiently support in-memory computing of Spconv3D and Conv2D. A weight workload balanced mechanism is proposed to mitigate the issue of workload

imbalance and improve computational resources utilization. Extensive experiments show that Voxel-CIM can achieve averagely 4.5~7.0× higher energy efficiency, 2.4~5.4× speed up in detection task and 1.2~8.1× speed up in segmentation task compared to the state-of-the-art point cloud accelerators and powerful GPUs.

ACKNOWLEDGMENTS

This work is supported in part by the National Natural Science Foundation of China (Grant No. 62304195), Guangzhou-HKUST(GZ) Joint Funding Program (No. 2024A03J0541), Guangzhou Municipal Science and Technology Project (Municipal Key Laboratory Construction Project, Grant No.2023A03J0013)

REFERENCES

- C. R. Qi, H. Su, K. Mo, and L. J. Guibas, “Pointnet: Deep learning on point sets for 3d classification and segmentation,” in *Proceedings of the IEEE conference on computer vision and pattern recognition*, 2017, pp. 652–660.
- C. R. Qi, L. Yi, H. Su, and L. J. Guibas, “Pointnet++: Deep hierarchical feature learning on point sets in a metric space,” *Advances in neural information processing systems*, vol. 30, 2017.
- T. Yin, X. Zhou, and P. Krahenbuhl, “Center-based 3d object detection and tracking,” in *Proceedings of the IEEE/CVF conference on computer vision and pattern recognition*, 2021, pp. 11 784–11 793.
- Y. Zhou and O. Tuzel, “Voxelnet: End-to-end learning for point cloud based 3d object detection,” in *Proceedings of the IEEE conference on computer vision and pattern recognition*, 2018, pp. 4490–4499.
- Y. Yan, Y. Mao, and B. Li, “Second: Sparsely embedded convolutional detection,” *Sensors*, vol. 18, no. 10, p. 3337, 2018.
- A. H. Lang, S. Vora, H. Caesar, L. Zhou, J. Yang, and O. Beijbom, “Pointpillars: Fast encoders for object detection from point clouds,” in *Proceedings of the IEEE/CVF conference on computer vision and pattern recognition*, 2019, pp. 12 697–12 705.
- S. Shi, C. Guo, L. Jiang, Z. Wang, J. Shi, X. Wang, and H. Li, “Pv-rcnn: Point-voxel feature set abstraction for 3d object detection,” in *Proceedings of the IEEE/CVF conference on computer vision and pattern recognition*, 2020, pp. 10 529–10 538.
- C. Choy, J. Gwak, and S. Savarese, “4d spatio-temporal convnets: Minkowski convolutional neural networks,” in *Proceedings of the IEEE/CVF conference on computer vision and pattern recognition*, 2019, pp. 3075–3084.
- D. Lyu, Z. Lil, Y. Chen, J. Zhang, N. Xu, and G. He, “Spocta: A 3d sparse convolution accelerator with octree-encoding-based map search and inherent sparsity-aware processing,” in *2023 IEEE/ACM International Conference on Computer Aided Design (ICCAD)*. IEEE, 2023, pp. 1–9.
- H. Tang, Z. Liu, S. Zhao, Y. Lin, J. Lin, H. Wang, and S. Han, “Searching efficient 3d architectures with sparse point-voxel convolution,” in *European conference on computer vision*. Springer, 2020, pp. 685–702.
- H. Tang, Z. Liu, X. Li, Y. Lin, and S. Han, “Torchsparse: Efficient point cloud inference engine,” *Proceedings of Machine Learning and Systems*, vol. 4, pp. 302–315, 2022.
- Q. Cao and J. Gu, “A sparse convolution neural network accelerator for 3d/4d point-cloud image recognition on low power mobile device with hopping-index rule book for efficient coordinate management,” in *2022 IEEE Symposium on VLSI Technology and Circuits (VLSI Technology and Circuits)*. IEEE, 2022, pp. 106–107.
- Y. Lin, Z. Zhang, H. Tang, H. Wang, and S. Han, “Pointacc: Efficient point cloud accelerator,” in *MICRO-54: 54th Annual IEEE/ACM International Symposium on Microarchitecture*, 2021, pp. 449–461.
- X. Yang, T. Fu, G. Dai, S. Zeng, K. Zhong, K. Hong, and Y. Wang, “An efficient accelerator for point-based and voxel-based point cloud neural networks,” in *2023 60th ACM/IEEE Design Automation Conference (DAC)*. IEEE, 2023, pp. 1–6.
- S. Yu, H. Jiang, S. Huang, X. Peng, and A. Lu, “Compute-in-memory chips for deep learning: Recent trends and prospects,” *IEEE circuits and systems magazine*, vol. 21, no. 3, pp. 31–56, 2021.
- K. Hong, Z. Yu, G. Dai, X. Yang, Y. Lian, N. Xu, and Y. Wang, “Exploiting hardware utilization and adaptive dataflow for efficient sparse convolution in 3d point clouds,” *Proceedings of Machine Learning and Systems*, vol. 5, 2023.
- B. Graham, M. Engelcke, and L. Van Der Maaten, “3d semantic segmentation with submanifold sparse convolutional networks,” in *Proceedings of the IEEE conference on computer vision and pattern recognition*, 2018, pp. 9224–9232.
- R. Girshick, “Fast r-cnn,” in *Proceedings of the IEEE international conference on computer vision*, 2015, pp. 1440–1448.
- T.-Y. Lin, P. Goyal, R. Girshick, K. He, and P. Dollár, “Focal loss for dense object detection,” in *Proceedings of the IEEE international conference on computer vision*, 2017, pp. 2980–2988.

- [20] T.-Y. Lin, P. Dollár, R. Girshick, K. He, B. Hariharan, and S. Belongie, “Feature pyramid networks for object detection,” in *Proceedings of the IEEE conference on computer vision and pattern recognition*, 2017, pp. 2117–2125.
- [21] traveller59, “second.pytorch,” 2019, GitHub repository. [Online]. Available: <https://github.com/traveller59/second.pytorch/issues/153>
- [22] L. Song, X. Qian, H. Li, and Y. Chen, “Piplayer: A pipelined reram-based accelerator for deep learning,” in *2017 IEEE international symposium on high performance computer architecture (HPCA)*. IEEE, 2017, pp. 541–552.
- [23] H. Jiang, S. Huang, X. Peng, and S. Yu, “Mint: Mixed-precision rram-based in-memory training architecture,” in *2020 IEEE International Symposium on Circuits and Systems (ISCAS)*. IEEE, 2020, pp. 1–5.
- [24] T. Yang, D. Li, Y. Han, Y. Zhao, F. Liu, X. Liang, Z. He, and L. Jiang, “Pimgcn: A reram-based pim design for graph convolutional network acceleration,” in *2021 58th ACM/IEEE Design Automation Conference (DAC)*. IEEE, 2021, pp. 583–588.
- [25] W. Li, X. Sun, S. Huang, H. Jiang, and S. Yu, “A 40-nm mlc-rram compute-in-memory macro with sparsity control, on-chip write-verify, and temperature-independent adc references,” *IEEE Journal of Solid-State Circuits*, vol. 57, no. 9, pp. 2868–2877, 2022.
- [26] X. Peng, R. Liu, and S. Yu, “Optimizing weight mapping and data flow for convolutional neural networks on rram based processing-in-memory architecture,” in *2019 IEEE International Symposium on Circuits and Systems (ISCAS)*. IEEE, 2019, pp. 1–5.
- [27] A. Geiger, P. Lenz, and R. Urtasun, “Are we ready for autonomous driving? the kitti vision benchmark suite,” in *2012 IEEE conference on computer vision and pattern recognition*. IEEE, 2012, pp. 3354–3361.
- [28] J. Behley, M. Garbade, A. Milioto, J. Quenzel, S. Behnke, C. Stachniss, and J. Gall, “Semantickitti: A dataset for semantic scene understanding of lidar sequences,” in *Proceedings of the IEEE/CVF international conference on computer vision*, 2019, pp. 9297–9307.
- [29] X. Peng, S. Huang, H. Jiang, A. Lu, and S. Yu, “Dnn+ neurosim v2. 0: An end-to-end benchmarking framework for compute-in-memory accelerators for on-chip training,” *IEEE Transactions on Computer-Aided Design of Integrated Circuits and Systems*, vol. 40, no. 11, pp. 2306–2319, 2020.
- [30] W. Sun, X. Feng, C. Tang, S. Fan, Y. Yang, J. Yue, H. Yang, and Y. Liu, “A 28nm 2d/3d unified sparse convolution accelerator with block-wise neighbor searcher for large-scaled voxel-based point cloud network,” in *2023 IEEE International Solid-State Circuits Conference (ISSCC)*. IEEE, 2023, pp. 328–330.